

Thermo-mechanical properties of mixed-matrix membranes encompassing zeolitic imidazolate framework-90 and polyvinylidene difluoride: ZIF-90/PVDF nanocomposites

Irina S. Flyagina, E. M. Mahdi, Kirill Titov, and Jin-Chong Tan^a

Multifunctional Materials & Composites (MMC) Laboratory, Department of Engineering Science, University of Oxford, Parks Road, Oxford OX1 3PJ, United Kingdom

(Received 6 June 2017; accepted 6 August 2017; published online 17 August 2017)

Mixed-matrix membranes are contemporary nanocomposite materials with many potential applications, from liquid and gas separations to chemical sensors and biomedicine. We report fabrication of a metal-organic framework (MOF)-based nanocomposite, combining polyvinylidene difluoride (PVDF) polymer as the matrix and ZIF-90 nanocrystals of up to 30 wt. % filler content. The focus is to establish the processing—microstructure—mechanical property relationships. We reveal the importance for quantifying salient effects of the filler contents: (i) tensile strength degrades beyond 10 wt. % and (ii) mechanical toughness declines due to membrane embrittlement. These are vital mechanical aspects but widely overlooked in the emergent field of MOF membranes and composites. © 2017 Author(s). All article content, except where otherwise noted, is licensed under a Creative Commons Attribution (CC BY) license (<http://creativecommons.org/licenses/by/4.0/>). [<http://dx.doi.org/10.1063/1.4986565>]

Contemporary economies require sustainable technologies that have high efficiency and reliability while implicating low environmental impact and small carbon footprint. Mixed-matrix membranes (MMMs) are versatile and very promising composite materials that can be utilized in many fields of application, for example, gas separation,^{1,2} liquid phase separation,^{3,4} pervaporation,⁵ and water desalination.⁶ A growing research area nowadays is carbon dioxide separation and its efficient removal from the environment leveraging membrane technologies in order to mitigate greenhouse effects.^{7,8} In the light of this, MMMs containing metal-organic frameworks (MOFs) as a functional filler offer tunable functionalities highly attractive for energy, sustainability, and environmental applications.^{9–11}

Research in the emerging field of MOF-based MMMs has been rapidly growing over the past decade.^{7,12} Typically, MOF-based MMMs are prepared by combining a solution of a polymer (matrix phase) and a dispersion of a MOF (filler phase), followed by solution casting the MOF/polymer film and solvent evaporation and/or heat treatment to achieve a free-standing composite membrane.¹³ Hitherto, there is little or no indication in the literature what rheological properties a MOF/polymer MMM dispersion should have before casting a good quality membrane. Particularly, there are only few studies dedicated to the detailed mechanical properties of MMMs, despite the fact that practical engineering applications¹⁴ will require mechanically robust membranes with long-term durability and good structural resilience.^{15–17}

Polyvinylidene difluoride (PVDF) is a semi-crystalline hydrophobic polymer with linear macromolecules¹⁸ and is reported as a promising material for liquid-soluble gas removal.^{3,19} PVDF has a good combination of mechanical properties and processing ability.²⁰ PVDF-based MMMs were reported to allow for high percentages of MOF loadings (>65 wt. %)²¹ as well as enhancing stability of MOFs in humid conditions.²²

MOF is a class of hybrid crystalline compounds built from organic-inorganic moieties, with a vast chemical and physical tunability to suit a wide range of applications.^{23–25} MOFs have attracted

^ajin-chong.tan@eng.ox.ac.uk

significant scientific attention due to its unique combination of properties: highly ordered intrinsic porosity and well-defined architecture, exceptionally large surface area, rich structural diversity, and facile synthesis methods.^{26–28} The filler phase used in this study is termed ZIF-90: belonging to a subclass of MOFs known as Zeolitic Imidazole Frameworks (ZIFs), it has a sodalite network topology and a high surface area ($1270 \text{ m}^2 \text{ g}^{-1}$),²⁹ akin to the prototypical ZIF-8 sodalite structure.^{30,31} While ZIF-90 is not as widely reported in the literature compared with ZIF-8, the former exhibits highly promising small-molecule selectivity to afford useful adsorption and diffusion applications.³²

In this work, we propose the fabrication of a novel MMM system comprising a PVDF matrix and ZIF-90 MOF fillers that can be potentially used for energy and sustainability applications. Herein, our emphasis is placed on the thermo-mechanical and physical properties of the MMMs, establishing the membrane compositions with tunable mechanical properties and to understand the structure-properties relationships. We achieved these employing X-ray diffraction and electron microscopy, combined with large-strain tensile testing, time- and temperature-dependent viscoelastic measurements, and nanoindentation studies. Additionally, we have considered the rheological properties of the pre-casting ZIF-90/PVDF dispersions to understand the basic conditions for guiding future membrane manufacturing.

Synthesis of ZIF-90: ZIF-90 nanoparticles were synthesized by following the procedure reported by Hua *et al.*³³ Briefly, zinc acetate dihydrate (Sigma Aldrich) and imidazole-2-carboxyaldehyde (ICA) (Sigma Aldrich) were taken in 1:8 molar ratio and dissolved in *N, N*-dimethylformamide (DMF) solvent. ICA was dissolved in a sufficient amount of DMF while magnetically stirred at 65 °C for 1 h. After cooling to the room temperature, zinc acetate solution was added to ICA dropwise under constant stirring, and the nanoparticles of ZIF-90 formed immediately. The reaction mixture was stirred for a few more hours to ensure that the reaction was completed. ZIF-90 was separated from the solvent by centrifugation (12 000 rpm for 1 h). To remove impurities, ZIF-90 was repeatedly re-dispersed in DMF by means of ultrasonication and separated in the centrifuge. Isolated nanoparticles were dried in a vacuum oven at 40 °C for at least 24 h.

Preparation of the MMMs: Four filler loadings of ZIF-90 in PVDF were obtained on the basis of weight percentages: 5, 10, 20, and 30 wt. %. First, PVDF powder with an averaged molecular weight of $M_w \sim 534\,000$ (Sigma Aldrich) was dissolved in DMF to obtain a 15.5 wt. % polymer solution. The required amounts of ZIF-90 nanoparticles were calculated using the equation,

$$\text{ZIF - 90 wt. \%} = \frac{m_{\text{ZIF - 90}}}{m_{\text{ZIF - 90}} + m_{\text{PVDF}}} \times 100\%, \quad (1)$$

where $m_{\text{ZIF-90}}$ is the mass of ZIF-90 nanoparticles and m_{PVDF} is the mass of the dry PVDF in its 15.5 wt. % solution in DMF. ZIF-90 was dispersed in 4 ml of acetone and ultrasonicated for 10 min, then combined with the required quantity of the PVDF solution and further ultrasonicated for a few hours to ensure thorough dispersion of ZIF-90 nanoparticles. To evaporate acetone and increase viscosity, the dispersions were further magnetically stirred on a hot plate at 50 °C. After degassing the dispersions by leaving unstirred overnight, the membranes were cast using the doctor-blade technique at a speed of 10 mm s^{-1} onto a glass substrate with the clearance set to 550 μm . Then the films were dried in an oven at 70 °C for ~ 20 min. The final thickness of the as-prepared membranes varied from ~ 40 to 60 μm . To remove DMF trapped in the ZIF-90/PVDF membranes, they were solvent-exchanged in methanol for a few days followed by vacuum-drying at 25 °C.

The cross sections of the ZIF-90/PVDF membranes were obtained by fracturing the samples in liquid nitrogen. The cross-sectional morphology was imaged (after carbon coated) using a field-emission scanning electron microscope (FESEM, Zeiss Merlin) at 1–3 keV. The ZIF-90 nanoparticles were imaged on transmission electron microscope (TEM) JEM-2100 LaB6 operating at 200 keV. The crystal structure of ZIF-90 and the membrane composition were determined by X-ray diffraction (XRD).

Thermal stability of the MMMs was investigated using TGA-Q50 (TA Instruments). The neat PVDF, membranes, and neat ZIF-90 were heated from 50 to 550 °C with a constant heating rate of $10 \text{ }^\circ\text{C min}^{-1}$ in a nitrogen atmosphere.

The uniaxial stress-strain curves (under tension) were obtained using the universal testing machine (Instron 5582) equipped with a 100 N load cell. The test coupons of 5 mm width, ~ 30 mm

gauge length, and 45–60 μm thickness were subjected to a tensile load applied at 2 mm min⁻¹ until fracture. For each MMM, 10–15 specimens were tested to achieve statistically meaningful results.

Instrumented nanoindentation measurements (under compression) were performed to obtain load-displacement curves and to quantify the Young modulus and hardness. A series of 20 indentations to a maximum depth of 2000 nm with a 50 μm interval was performed for each of the MMMs on the MTS NanoIndenter XP (Agilent Technologies), equipped with a Berkovich three-sided pyramid indenter tip. We applied the continuous stiffness measurement (CSM) method, with a loading and unloading strain rate of 0.05 s⁻¹ at 45 Hz.^{34,35}

Temperature-dependent viscoelastic properties were characterized using DMA-Q800 (TA Instruments) connected to a liquid nitrogen tank via flow-controller to acquire data from low temperatures. The DMA was calibrated to a pair of tension clamps with a fixed gauge length of 12.5 mm. The test coupons of the MMMs of 5 mm width and thickness varying in the range of 45–60 μm were tested under uniaxial tensile mode (small strain 0.1%) with oscillating frequencies of 2, 5, 10, 15, 20, 30, 35, and 40 Hz in a temperature range from -80 to 150 °C. The heating rate was 2 °C min⁻¹, the static force was set at 0.1 N, and the force track was set to 125%. For each MMM, 4–7 specimens were tested to ensure sufficient data reproducibility.

Figure 1(a) shows the prepared ZIF-90/PVDF nanocomposite membranes, while the XRD patterns and TGA curves of ZIF-90 nanoparticles and MMMs are presented in Figs. 1(b) and 1(c), respectively. The XRD diffraction patterns confirm that the synthesis and incorporation of ZIF-90 nanoparticles into the PVDF polymer matrix were successful. The characteristic peaks of PVDF are

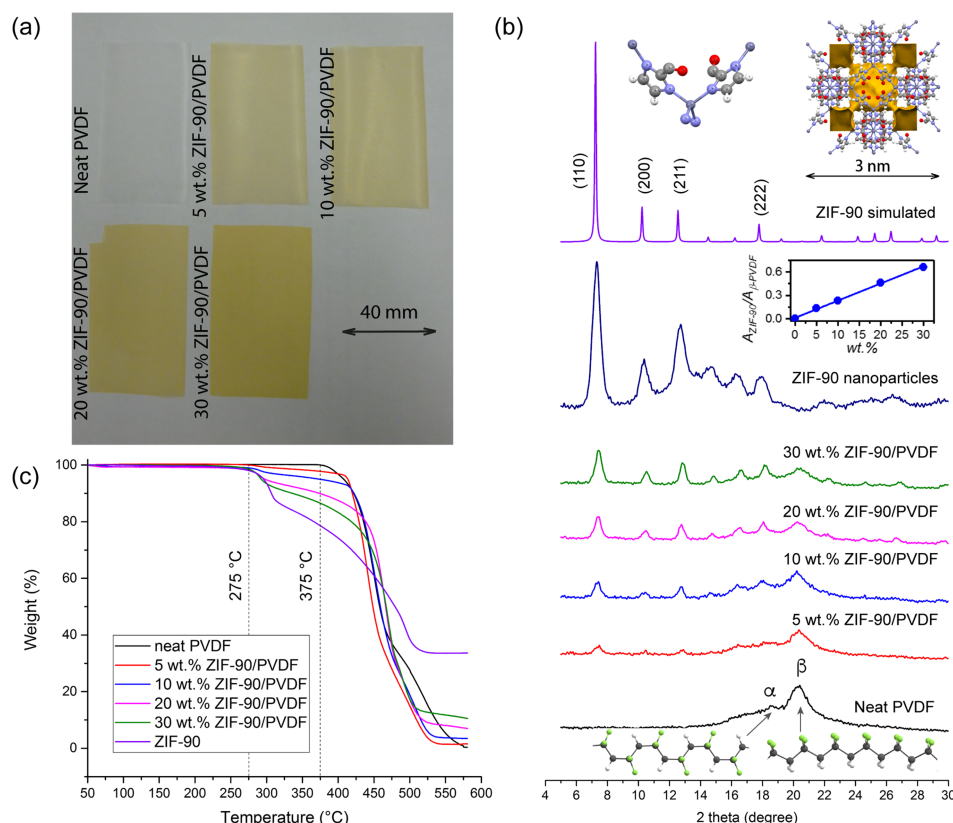


FIG. 1. (a) Photographs of the nanocomposite membranes prepared in this study, (b) XRD patterns of ZIF-90, neat PVDF, and the MMMs, and (c) TGA results. The molecular structures of ZIF-90 (asymmetric unit and pore packing per unit cell, where yellow surface represents the solvent accessible volume) and α - and β - crystalline phases of PVDF are shown next to the corresponding XRD patterns. The inset shows the excellent correlation between the integrated intensities of relative peak areas [ZIF-90's (110) planes normalized by PVDF's β -phase] against the wt. % content of the ZIF-90 nanoparticles. The C, O, N, Zn, H, and F atoms are designated in grey, red, lilac, dark-lilac, white, and green colors, respectively.

at $2\theta = 17.66^\circ$, 18.30° , 19.90° , and 26.56° for the α and γ phases and at 20.26° for the β phase.¹⁸ The pronounced peak at $2\theta \approx 20.3^\circ$ indicates that the PVDF in the MMMs is semi-crystalline, containing predominantly the β phase. In the case of ZIF-90, the observed peaks measured at $2\theta \approx 7.3^\circ$, 10.4° , 14.8° , 16.5° , and 17.9° are in excellent agreement with the simulated diffraction pattern of an ideal single crystal; the peak broadening observed is characteristic of the nanosized crystalline material. It can be seen in Fig. 1(b) that the three major peaks of ZIF-90 in the MMMs, specifically the intensities of (110), (200), and (211) crystallographic planes are scaling with the wt. % loading of the ZIF-90 filler phase.

Thermal stability of the ZIF-90/PVDF MMMs as well as the neat PVDF membrane and ZIF-90 nanoparticles were characterized by thermogravimetric analysis (TGA). TGA data in Fig. 1(c) suggest that the neat PVDF starts to decompose rapidly beyond 375°C . In contrast, ZIF-90 starts to decompose at a relatively lower temperature of 275°C . Since no weight loss was observed at temperatures lower than these points, residual solvents (DMF, methanol, water) were completely removed after solvent exchange and evacuation. Between 275 and 375°C , a systematic trend exists where the thermal stability of the ZIF-90/PVDF nanocomposite is gradually decreasing with an increasing ZIF-90 loading from 5 to 30 wt. %. The TGA results suggest that there are intimate MOF-to-polymer coupling interactions, attributable to the chemical affinity of the organic ICA linkers of ZIF-90 to adjacent macromolecules in the PVDF matrix.

The morphologies of ZIF-90 nanoparticles and the cross sections of MMMs are shown in Fig. 2. The average particle size of the as-synthesized ZIF-90 was ~ 100 nm [Fig. 2(a)]; the TEM image in the inset reveals that individual nanoparticle does not exhibit well defined crystal facets (unlike ZIF-8 nanoparticles)¹⁷ due to twinning and nanocrystalline intergrowth. The nanoparticle distribution in the PVDF matrix appears to be uniform, evidenced in the 20 wt. % and 30 wt. % nanocomposites shown in Figs. 2(e) and 2(f); the nanoparticles are also well encapsulated by the matrix phase. This was achieved by thorough dispersion of ZIF-90 in PVDF solution and by controlling the viscosity of the mixture for an improved particle distribution. We found that the viscosity of ~ 1 Pa s is sufficient to maintain a uniform suspension of nanoparticles in the PVDF solution and to facilitate membrane casting using the doctor-blade approach (see Figs. S1-S3 of the [supplementary material](#)).

Tensile testing is a primary technique for determination of the mechanical properties of engineering materials, such as the Young modulus (E), yield and tensile strengths, fracture energy,

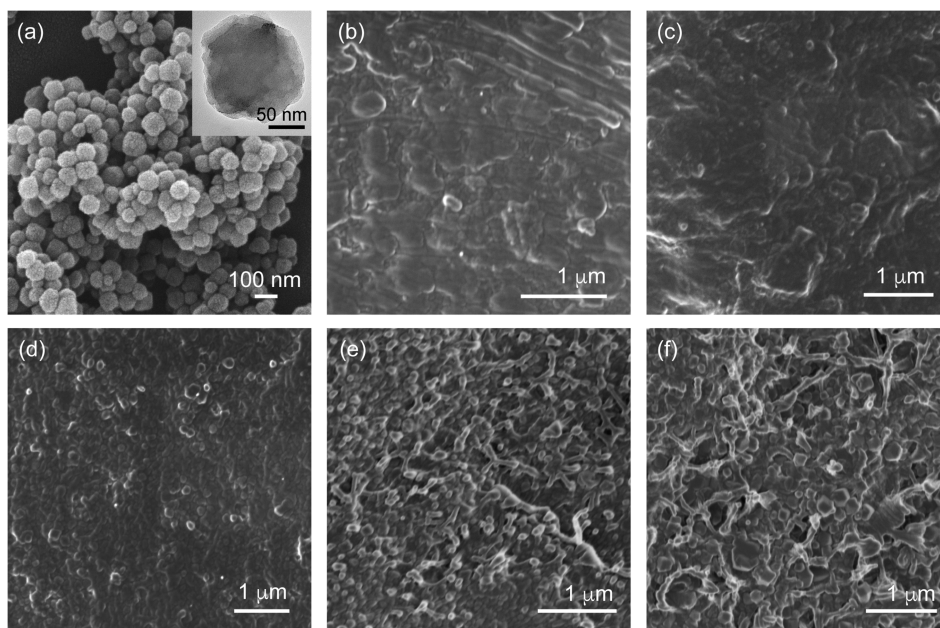


FIG. 2. FESEM micrographs of (a) ZIF-90 with the TEM image inset and the membrane cross sections of (b) neat PVDF, (c) 5 wt. %, (d) 10 wt. %, (e) 20 wt. %, and (f) 30 wt. % ZIF-90/PVDF.

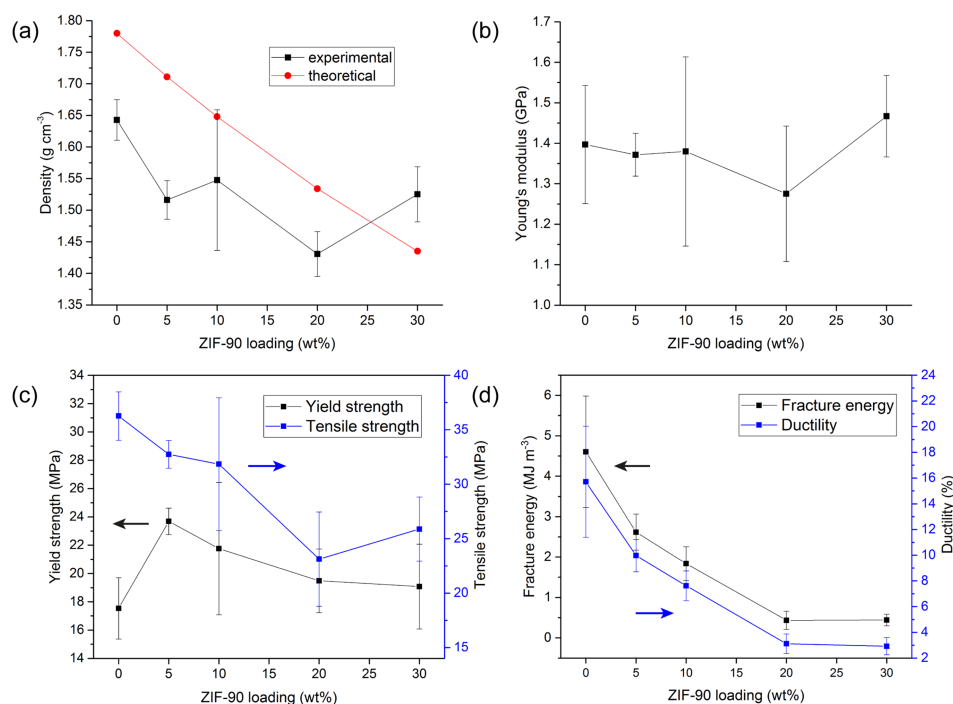


FIG. 3. (a) Density, (b) Young modulus E , (c) yield strength at 0.2% strain offset and tensile strength, (d) fracture energy and ductility of the ZIF-90/PVDF MMMs as a function of the ZIF-90 wt. % loading. Uniaxial tensile tests were performed at 2 mm min^{-1} , each involving 10-15 samples (Fig. S5 of the [supplementary material](#)).

and ductility (elongation-to-failure %). These key mechanical properties, summarized in Fig. 3, were derived from a series of stress-strain curves obtained from uniaxial tensile tests (Fig. S5 of the [supplementary material](#)). In Fig. 3(a), the density of the tested membrane samples was measured and compared with theoretical values calculated based on the density of the neat matrix and filler components (by taking $\rho_{\text{PVDF}} = 1.78 \text{ g cm}^{-3}$ and $\rho_{\text{ZIF-90}} = 0.988 \text{ g cm}^{-3}$) and wt. % loadings of ZIF-90 in the composites. The experimentally measured densities are lower than the theoretically estimated values for most of the membranes, which indicates presence of some free volume in the MMMs.

The Young moduli (a measure of elastic stiffness) of the MMMs derived from uniaxial tensile tests are shown in Fig. 3(b), found to be at $\sim 1.4 \text{ GPa}$ and appeared to be independent of wt. % loading of the ZIF-90 nanoparticles. Here it is worth noting that this stiffness value is likely to be underestimated from the tensile test (which is a well-known issue),³⁶ thus in Fig. 4 we applied nanoindentation to better characterize the elastic stiffness property. Results in Fig. 3(c) show that the yield strength of PVDF ($\sim 18 \text{ MPa}$) increases upon addition of 5 wt. % ZIF-90, followed by a gradual decline from ~ 24 to $\sim 20 \text{ MPa}$ when the filler content was raised from 10 to 30 wt. %. The tensile strength of membranes decreased from ~ 36 to $\sim 26 \text{ MPa}$, which is reasonable, since the higher loadings of ZIF-90 resulted in increasing embrittlement of the MMMs as indicated by the reduction in the sample ductility. On this basis, the fracture energy (integrated area under the nominal stress-strain curve, i.e., energy per unit volume) decreases systematically with the fall in sample ductility as presented in Fig. 3(d). Specifically, we found the fracture energy of the neat PVDF membrane declined by $\sim 90\%$ upon the addition of 30 wt. % of ZIF-90, resulting from the ductility drop of $\sim 80\%$. Importantly, these results indicate that in order to achieve a mechanically resilient MMM exhibiting good toughness property, a MOF filler content of $\sim 5\text{-}10 \text{ wt. \%}$ is likely to be optimal. Higher filler contents, however, will lead to an unwanted embrittlement of the composite, thus diminishing the ductility and toughness properties leading to the membrane cracking. Indeed, this finding is consistent with our previous studies utilizing glassy Matrimid as a matrix to support ZIF-8 nanoparticles.¹⁶

To investigate the fine-scale mechanical properties of the ZIF-90/PVDF MMMs, we performed instrumented nanoindentation experiments to quantify the indentation modulus and hardness as a function of the ZIF-90 wt. % filler content. The measured load-displacement curves of the MMMs

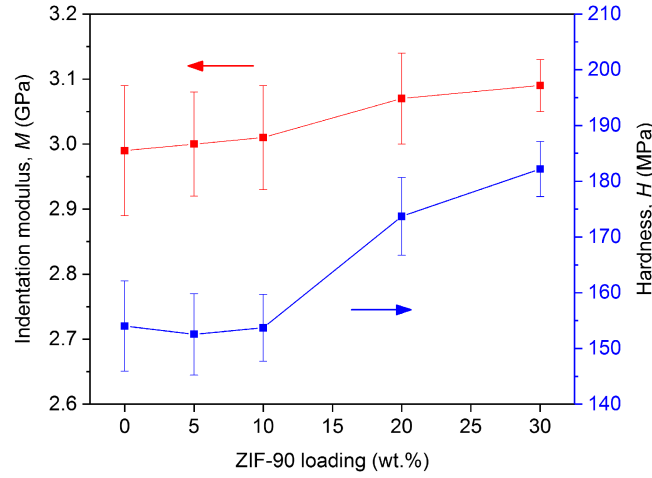


FIG. 4. Indentation modulus (M) and hardness (H) of the ZIF-90/PVDF MMM (top surface) determined using the instrumented nanoindentation method. Each averaged value and standard deviation corresponds to 15–20 indentation measurements derived from a surface penetration depth of 200–2000 nm (refer to Figs. S6 and S7 of the [supplementary material](#) for further details).

for a maximum surface penetration depth of 2 μm are presented in Fig. S6 ([supplementary material](#)). The indentation modulus (M) and hardness (H) values have been derived from the nanoindentation curves, in accordance with Eqs. (2) and (3), respectively,³⁷

$$M = \left[\frac{1}{E_r} - \frac{1 - \nu_i^2}{E_i} \right]^{-1}, \quad (2)$$

$$H = \frac{P}{A_c}, \quad (3)$$

where E_r is the reduced modulus,³⁸ E_i and ν_i are the Young modulus and the Poisson ratio of the diamond indenter tip (whose values are 1141 GPa and 0.07, respectively). P is the indentation load as a function of the surface penetration depth and A_c is the contact area developed under that load.

It can be seen in Fig. 4 that the indentation moduli (a measure of stiffness) of the MMMs are lying in the narrow range of 2.9–3.1 GPa, indicating that the stiffness of ZIF-90 is similar in magnitude to that of the PVDF matrix. Thus, mixing of the two constituent phases did not significantly alter the resulting stiffness of the composite. On the contrary, there is a clear rise in the membrane hardness especially beyond 10 wt. %, from $H \sim 150$ MPa for the neat PVDF membrane to ~ 185 MPa for the 30 wt. % ZIF-90/PVDF. This indicates that the hardness of ZIF-90 is notably higher than that of the neat PVDF phase. Assuming that the composite obeys the rule of mixtures relation (in equal strain),^{16,39} we estimated the hardness of ZIF-90 to be ~ 250 MPa, which is only about half of its sodalite counterpart ZIF-8, whose hardness is ~ 530 MPa.⁴⁰

The Young modulus of the membrane (subscript m) can be estimated using the following relation,⁴¹ if its Poisson ratio is known and assumed to be isotropic,

$$E_m = M (1 - \nu_m^2), \quad (4)$$

where M is the indentation modulus given by Eq. (2) and ν_m is the Poisson ratio of the membrane.

Equation (4) above is a good approximation for the neat PVDF membrane. Taking $\nu_m = 0.34$,⁴² we estimated the Young modulus of the neat PVDF membrane (thickness ~ 50 μm) to be 2.65 ± 0.09 GPa, which is in good agreement with the recent literature values (e.g., $E = 2.5$ – 2.7 GPa from Ref. 42; $E = 2.5$ GPa from Ref. 43).

Dynamic mechanical analysis (DMA) has become a standard method of investigating the viscoelastic properties of polymers.^{16,17} In this study, we focused on characterizing the temperature-dependent storage and loss moduli of the MMMs to understand the effects of MOF filler inclusion.

In the DMA theory, for a material subject to a cyclic deformation, the storage modulus (E') is a measure of its elastic behavior (i.e., stored energy) that is responsible for its time-dependent recovery, while the loss modulus (E'') is a measure of the viscous behavior responsible for its irreversible energy dissipation. The ratio of these two quantities is termed the loss tangent, defined as $\tan \delta = E''/E'$, where phase transition temperatures can be pinpointed by locating the position of the $\tan(\delta)$ peaks via a temperature-sweep experiment.

The storage and loss moduli of the MMMs measured from -80 to 160 °C are presented in Figs. 5(a) and 5(b), respectively. The general trend reveals that the magnitude of both E' and E'' has systematically declined, with an increasingly higher wt. % of ZIF-90 filler being added into the neat PVDF matrix. The DMA data indicate that incorporation of the relatively compliant porous ZIF nanocrystals⁴⁴ into the PVDF matrix has reduced the energy storage capacity of the composite when subject to an oscillatory strain, thus E' decreases. We reasoned that the increasing filler content may have caused rigidification of the PVDF macromolecules in the vicinity of each nanoparticle, thereby reducing the energy dissipation capacity of the MMMs, as quantified by E'' . Taken together, the ratio of E''/E' which corresponds to the loss tangent [see the inset of Fig. 5(b) for $\tan \delta$ values] fell with the rising filler contents. This means that the dampening capacity of the MMMs can be modified by tuning the filler wt. %. We also found that the magnitude of the glass transition temperature ($T_g = -40$ °C) is not sensitive to the addition of the ZIF-90 fillers. Figures 5(c) and 5(d) summarize the variation in storage and loss moduli as a function of the ZIF-90 wt. %, at $T_g = -40$ °C and at room temperature $RT = 25$ °C, respectively. It can be seen that the storage modulus has decreased gradually from the neat PVDF to the 20 wt. % ZIF-90/PVDF: by 44% at -40 °C and by 33% at 25 °C; a similar trend can be observed for the corresponding loss moduli.

In summary, a novel mixed-matrix nanocomposite membrane comprising PVDF as the polymer matrix and ZIF-90 nanoparticles as a filler has been fabricated, and its physical and mechanical properties have been systematically characterized. Our main findings are:

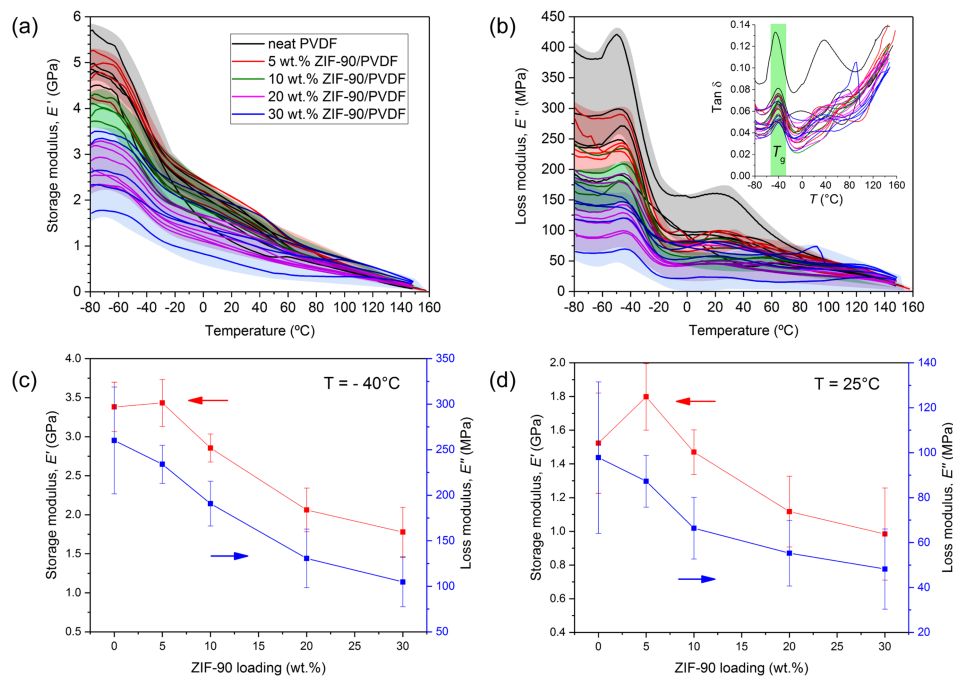


FIG. 5. DMA curves for the neat PVDF and ZIF-90/PVDF MMMs tested under the tensile mode: (a) storage modulus E' and (b) loss modulus E'' with the inset showing the loss tangent ($\tan \delta = E''/E'$). The bands illustrate the material variability between specimens with the same ZIF-90 wt. % loading. Variation of E' and E'' as a function of temperature at (c) glass transition temperature, $T_g = -40$ °C and (d) room temperature 25 °C. Further details can be found in the [supplementary material](#), see Figs. S8-S10.

- Rheological studies of the ZIF-90/PVDF composite solution suggest a minimum viscosity of ~ 1 Pa s to ensure stability of the filler dispersion and ease of membrane processing via doctor blade or tape casting.
- For quasistatic mechanical behavior, the elastic stiffness is nearly independent of the wt. % of ZIF-90, while the indentation hardness shows a stronger scaling with filler content.
- Large strain mechanical deformation studies reveal that higher than ~ 10 wt. % loadings cause a major loss of tensile strength and embrittlement, degrading the durability of the membranes.
- Dynamic mechanical data at a small oscillatory strain show that the glass transition temperature of PVDF is not affected by the filler inclusion. However, both the storage and loss moduli systematically decline with an increasing filler content.
- There is an opportunity to tune the energy storage (E') and energy dissipation (E'') characteristics of the MOF/Polymer MMMs to tailor the viscoelasticity of nanocomposite systems for applications requiring cyclic mechanical deformation.

See [supplementary material](#) for detailed data obtained from rheological measurements, uniaxial tensile tests, nanoindentation, and dynamic mechanical analysis. It also contains additional scanning electron microscopy images of the membrane cross sections. Additional data can be accessed via ORA (<http://ora.ouls.ox.ac.uk>). Request for any material samples described in this manuscript can be directed to the corresponding author.

This work was supported by the EPSRC Grant No. EP/N014960/1. The authors would like to acknowledge the Research Complex at Harwell (RCAH) for access to the materials characterization facilities; particular thanks are to Dr. James Gilchrist for assistance and training in acquiring the TEM images. We are grateful to Dr. Gavin Stenning and Dr. Marek Jura at R53 Materials Characterization Laboratory (ISIS Rutherford Appleton Laboratories) for providing access to the XRD facilities. Additionally, I. S. Flyagina would like to thank Dr. Detlev C. Mielczarek (IFP Energies Nouvelles) for his help in the design of the illustrations.

- ¹ J. E. Bachman, Z. P. Smith, T. Li, T. Xu, and J. R. Long, *Nat. Mater.* **15**(8), 845–849 (2016).
- ² T. Watanabe and D. S. Sholl, *Langmuir* **28**(40), 14114–14128 (2012).
- ³ R. Naim, A. F. Ismail, and A. Mansourizadeh, *J. Membr. Sci.* **392**, 29–37 (2012).
- ⁴ S. Kaur, S. Sundararajan, D. Rana, R. Sridhar, R. Gopal, T. Matsuura, and S. Ramakrishna, *J. Mater. Sci.* **49**(18), 6143–6159 (2014).
- ⁵ Y. H. Deng, J. T. Chen, C. H. Chang, K. S. Liao, K. L. Tung, W. E. Price, Y. Yamauchi, and K. C. Wu, *Angew. Chem., Int. Ed.* **55**(41), 12793–12796 (2016).
- ⁶ D. Y. Hou, J. Wang, X. C. Sun, Z. G. Ji, and Z. K. Luan, *J. Membr. Sci.* **405**, 185–200 (2012).
- ⁷ B. Seoane, J. Coronas, I. Gascon, M. E. Benavides, O. Karvan, J. Caro, F. Kapteijn, and J. Gascon, *Chem. Soc. Rev.* **44**(8), 2421–2454 (2015).
- ⁸ I. Erucar and S. Keskin, *Ind. Eng. Chem. Res.* **52**(9), 3462–3472 (2013).
- ⁹ W. J. Koros and C. Zhang, *Nat. Mater.* **16**(3), 289–297 (2017).
- ¹⁰ E. M. Mahdi, A. K. Chaudhuri, and J. C. Tan, *Mol. Syst. Des. Eng.* **1**(1), 122–131 (2016).
- ¹¹ G. X. Dong, H. Y. Li, and V. K. Chen, *J. Mater. Chem. A* **1**(15), 4610–4630 (2013).
- ¹² B. Zornoza, C. Tellez, J. Coronas, J. Gascon, and F. Kapteijn, *Microporous Mesoporous Mater.* **166**, 67–78 (2013).
- ¹³ M. J. C. Ordoñez, K. J. Balkus, J. P. Ferraris, and I. H. Musselman, *J. Membr. Sci.* **361**(1–2), 28–37 (2010).
- ¹⁴ J. Caro, *Curr. Opin. Chem. Eng.* **1**(1), 77–83 (2011).
- ¹⁵ S. J. D. Smith, C. H. Lau, J. I. Mardel, M. Kitchin, K. Konstas, B. P. Ladewig, and M. R. Hill, *J. Mater. Chem. A* **4**, 10627–10634 (2016).
- ¹⁶ E. M. Mahdi and J. C. Tan, *J. Membr. Sci.* **498**, 276–290 (2016).
- ¹⁷ E. M. Mahdi and J. C. Tan, *Polymer* **97**, 31–43 (2016).
- ¹⁸ D. L. Yang, S. Tornga, B. Orler, and C. Welch, *J. Membr. Sci.* **409**, 302–317 (2012).
- ¹⁹ K. Li, J. F. Kong, D. L. Wang, and W. K. Teo, *AIChE J.* **45**(6), 1211–1219 (1999).
- ²⁰ X. G. Tang, M. Hou, L. Ge, J. Zou, R. Truss, W. Yang, M. B. Yang, Z. H. Zhu, and R. Y. Bao, *J. Appl. Polym. Sci.* **125**, E592–E600 (2012).
- ²¹ M. S. Denny, Jr. and S. M. Cohen, *Angew. Chem., Int. Ed.* **54**(31), 9029–9032 (2015).
- ²² J. B. DeCoste, J. M. S. Denny, G. W. Peterson, J. J. Mahle, and S. M. Cohen, *Chem. Sci.* **7**(4), 2711–2716 (2016).
- ²³ G. Maurin, C. Serre, A. Cooper, and G. Férey, *Chem. Soc. Rev.* **46**, 3104–3107 (2017).
- ²⁴ J. C. Tan and B. Civalieri, *CrystEngComm* **17**(2), 197–198 (2015).
- ²⁵ W. Li, S. Henke, and A. K. Cheetham, *APL Mater.* **2**(12), 123902 (2014).
- ²⁶ K. Sumida, K. Liang, J. Reboul, I. A. Ibarra, S. Furukawa, and P. Falcaro, *Chem. Mater.* **29**(7), 2626–2645 (2017).
- ²⁷ N. Stock and S. Biswas, *Chem. Rev.* **112**(2), 933–969 (2012).
- ²⁸ M. R. Ryder and J. C. Tan, *Mater. Sci. Technol.* **30**(13A), 1598–1612 (2014).
- ²⁹ W. Morris, C. J. Doonan, H. Furukawa, R. Banerjee, and O. M. Yaghi, *J. Am. Chem. Soc.* **130**(38), 12626–12627 (2008).

- ³⁰ A. Phan, C. J. Doonan, F. J. Uribe-Romo, C. B. Knobler, M. O’Keeffe, and O. M. Yaghi, *Acc. Chem. Res.* **43**(1), 58–67 (2010).
- ³¹ J. C. Tan, B. Civalleri, C. C. Lin, L. Valenzano, R. Galvelis, P. F. Chen, T. D. Bennett, C. Mellot-Draznieks, C. M. Zicovich-Wilson, and A. K. Cheetham, *Phys. Rev. Lett.* **108**(9), 095502 (2012).
- ³² J. A. Gee, J. Chung, S. Nair, and D. S. Sholl, *J. Phys. Chem. C* **117**(6), 3169–3176 (2013).
- ³³ D. Hua, Y. K. Ong, Y. Wang, T. Yang, and T.-S. Chung, *J. Membr. Sci.* **453**, 155–167 (2014).
- ³⁴ J. C. Tan, J. D. Furman, and A. K. Cheetham, *J. Am. Chem. Soc.* **131**(40), 14252–14254 (2009).
- ³⁵ M. Kosa, J. C. Tan, C. A. Merrill, M. Krack, A. K. Cheetham, and M. Parrinello, *ChemPhysChem* **11**(11), 2332–2336 (2010).
- ³⁶ J. D. Lord and R. M. Morrell, *Metrologia* **47**(2), S41–S49 (2010).
- ³⁷ W. C. Oliver and G. M. Pharr, *J. Mater. Res.* **7**(6), 1564–1583 (1992).
- ³⁸ J. Hay, *Exp. Tech.* **33**(6), 66–72 (2009).
- ³⁹ D. Hull and T. W. Clyne, *An Introduction to Composite Materials* (Cambridge University Press, 1996).
- ⁴⁰ N. W. Khun, E. M. Mahdi, S. Q. Ying, T. Sui, A. M. Korsunsky, and J. C. Tan, *APL Mater.* **2**(12), 124101 (2014).
- ⁴¹ J. C. Tan, C. A. Merrill, J. B. Orton, and A. K. Cheetham, *Acta Mater.* **57**(12), 3481–3496 (2009).
- ⁴² A. Vinogradov and F. Holloway, *Ferroelectrics* **226**(1-4), 169–181 (1999).
- ⁴³ B. Mohammadi, A. A. Yousefi, and S. M. Bellah, *Polym. Test.* **26**(1), 42–50 (2007).
- ⁴⁴ J. C. Tan, T. D. Bennett, and A. K. Cheetham, *Proc. Natl. Acad. Sci. U. S. A.* **107**(22), 9938–9943 (2010).